tions ensures bounded solutions so that we focus on oscillatory solutions and their sensitivity to changes in the parameters. The reference case shows how an initial small perturbation slowly amplifies before settling down to an oscillation with a period of 35 years and an amplitude of about 1°C (Fig. 4A). The tropical and extratropical fluctuations are out of phase. A cycle starts with a rapid increase in equatorial temperatures (because of the local positive feedback). It causes a drop in extratropical surface temperature as a result of an intensification of the extratropical westerly winds and enhanced evaporation. The increased latitudinal temperature difference gives rise to a poleward transport of heat that halts both the warming of the tropics and the cooling of the extratropics, establishing an equilibrium state that persists for a considerable time before coming to an end and entering into the complementary phase. The period of the oscillation is determined mainly by the delay time d, which depends on the time it takes parcels to travel from the surface in the extratropics to the equator. In reality, no single value can be assigned to d because surface water subducts over a wide range of latitudes and because there are various routes a parcel can follow to reach the equator (Fig. 2). This suggest a broad-band spectrum for interdecadal climate fluctuations.

In Fig. 4A, the oscillation is perfectly periodic and transitions from one phase to the other are very abrupt. The introduction of stochastic forcing in the extratropics (Fig. 4, B and C) causes the transition to be more gradual. Calculations to explore the sensitivity of the results to specified parameters reveal that the period of the oscillation depends linearly on d. A change in γ, which determines the rate at which heat is transported poleward, affects the magnitude but not the period of the oscillation. Changes in the feedback parameters λ_1 and λ_2 effect bifurcations that correspond to discontinuous changes in the period of the oscillation.

The results presented here demonstrate that it is in principle possible for links between the extratropics and the tropics—rapid and poleward in the atmosphere, slow and equatorward in the ocean—to cause continual interdecadal climate fluctuations. Further studies, observational ones such as the analysis by Zhang *et al.* (*13*) and theoretical ones, are needed to determine the detailed structure of these fluctuations and of the processes, such as oceanic subduction, on which they depend.

REFERENCES AND NOTES

1. S. G. H. Philander, *El Niño, La Niña, and the Southern Oscillation* (Academic Press, New York, 1990); D. Neelin *et al.*, *Annu. Rev. Fluid Mech.* **26**, 617 (1994).
2. D. Gu and S. G. H. Philander, *J. Clim.* **8**, 864 (1995); K. Trenberth and T. J. Hoar, *Geophys. Res. Lett.* **23**, 57 (1996); T. Knutson, S. Manabe, D. Gu, *J. Clim.*, in press.
3. M. Latif *et al.*, *Clim. Dyn.* **9**, 167 (1994).
4. M. Ji *et al.*, *J. Clim.* **9**, 3105 (1996).
5. This statement does not exclude exchanges between the narrow equatorial zone and the neighboring region that cause variations in the mean depth of the thermocline, primarily within the tropics. F.-F. Jin [*Science* **274**, 76 (1996)] discusses such exchanges.
6. D. Gu, S. G. H. Philander, M. McPhaden, in preparation.
7. R. A. Fine *et al.*, *J. Phys. Oceanogr.* **17**, 553 (1987).
8. Z. Liu and S. G. H. Philander, *ibid.* **25**, 449 (1995); Z. Liu *et al.*, *ibid.* **24**, 2606 (1994); P. Lu and J. P. McCreary, *ibid.* **25**, 2606 (1995).
9. C. Deser, M. A. Alexander, M. S. Timlin, *J. Clim.* **9**, 1840 (1996).
10. N.-C. Lau and M. Nath, *ibid.* **7**, 1184 (1994); K. Trenberth and J. W. Hurrell, *Clim. Dyn.* **9**, 303 (1994).
11. M. Latif and T. P. Barnett, *Science* **266**, 634 (1994).
12. Equations similar to Eqs. 2, 3, and 4 have been discussed in connection with a delayed oscillator theory for El Niño and the Southern Oscillation. See, for example, P. S. Schopf and M. J. Suarez, *J. Atmos. Sci.* **45**, 549 (1988); for a more general discussion, see L. Gyori and G. Ladas, *Oscillation Theory of Delay Differential Equations* (Oxford Univ. Press, Oxford, 1991).
13. Y. Zhang, J. M. Wallace, D. S. Battisti, *J. Clim.*, in press.
14. M. J. McPhaden, *Oceanography* **2**, 36 (1993).

15. We benefited from discussions with K. Bryan, A. Bush, T. Delworth, I. Held, M. Latif, N.-C. Lau, S. Manabe, I. Orlanski, and R. Toggweiler. S. Harper provided Fig. 2; M. McPhaden provided data for Fig. 1. This research was supported by NOAA under contract NOAA-NA56GP0226 and by NASA under contract UCLA-NASA-NAG5-2224.

20 September 1996; accepted 13 December 1996

Numerical Simulation of the Cretaceous Tethys Circumglobal Current

Andrew B. G. Bush

Certain paleobiogeographical reconstructions of ocean currents during the Cretaceous (about 144 to 65 million years ago) suggest that a circumglobal tropical current flowed westward through the continental configuration of that time. Although some numerical climate models failed in initial attempts to simulate this current, simulations with a coupled atmosphere-ocean model with relatively high spatial resolution and a late Cretaceous continental distribution show that a circumglobal current is a robust feature even though local surface currents in the Tethys Seaway reverse during the south Eurasian monsoon months.

The continuously changing shapes and positions of continents significantly influence the evolution and migration of life on the planet. One of the most important mammal migrations occurred during the early to mid-Miocene [~23.2 to 11.8 million years ago (Ma)] when collision of the Arabian and Turkish plates formed a land bridge between Africa and Eurasia (*1*). This collision also effectively closed the Mediterranean-Indonesian seaway, thereby blocking from that time until the present a circumglobal pathway in which flowed, it is hypothesized, a warm, saline current (*2–4*).

This westward-flowing Tethys circumglobal current (TCC) is believed to have contributed to tropical climates from 30°S to 30°N from the Triassic through the Cretaceous (~245 to 65 Ma) (*5*). Its demise in the Miocene was associated with a substantial climate change to the coastal regions of the southern Tethys Ocean, including northwest Africa, northern South America, southern North America, and western Eurasia (*2*). This climate change had a fundamental impact on the flora and fauna of these regions: For example, vegetation in North America transformed from that of a tropical rain forest in the Eocene (~55 to 34 Ma) to that of a savanna in the Miocene (*6*).

The failure of a recent numerical simulation of the mid-Cretaceous ocean to reproduce such a circumglobal, westward-flowing, equatorial current led to increased scrutiny of the geological evidence and to a controversy concerning the very existence of the TCC (*7*). In the simulations, the Tethys Ocean has prominent eastward currents—part of the wind-driven gyre circulation—but no westward return flow indicative of a TCC along the continental margins of southern Eurasia, Africa, or South America (*8, 9*). This discrepancy between biogeographic evidence and modeling efforts was attributed to the absence of a poleward shift of the mid-latitude westerly winds in the simulation, a shift which had previously been an assumed feature of an ice-free planet in the reconstructions (*8, 10*).

This report describes a numerical simulation that has the TCC as a robust feature of the late Cretaceous ocean circulation. We used an atmospheric general circulation model (GCM) (*11*) that is dynamically and thermodynamically coupled to an oceanic

Atmospheric and Oceanic Sciences Program, Princeton University, Post Office Box CN710, Sayre Hall, Princeton, NJ 08544–0710, USA.

GCM (*12*). In a slightly different configuration, this coupled model has been used to describe the atmosphere-ocean response to, for example, CO_2 variations (*13*) and anomalous freshwater fluxes in the North Atlantic (*14*). In the atmospheric model, we quadrupled the present-day value for the mixing ratio of atmospheric CO_2 to be indicative of proposed CO_2 levels during the Cretaceous (*15*). We adopted a paleogeographical reconstruction for the Maestrichtian Stage of the late Cretaceous (*16*). The atmospheric model used a spectral representation of variables with a wave number truncation that delivers an equivalent Gaussian resolution of 3.75° in longitude and 2.25° in latitude; the ocean model was formulated by finite-difference methods and has a spatial grid of 3.62° in longitude and 2° in latitude, along with 15 unevenly spaced levels in the vertical. We imposed seasonally varying solar radiative forcing with orbital parameters equivalent to those of the present day.

Coupling between the two models proceeded in intervals of 1 day. The atmospheric model delivered surface boundary conditions for the ocean model in the form of zonal and meridional wind stress, heat flux, freshwater flux, and net shortwave radiation. In turn, the ocean model delivered to the atmospheric model surface current velocities and sea surface temperature (SST). Because the model's climatology is reasonable for the decadal time scales of the wind-driven circulation, we did not apply any flux correction during the integration.

We integrated the equations for a model duration of 32 years starting from an ocean that was initially at rest with a thermal (and saline) structure that was a prescribed function of latitude and depth. Because the incoming solar radiation was equal to that of today and because in the absence of dynamics it is the radiative forcing that determines the meridional structure of the ocean's temperature, this function was taken to be a zonal average of the present-day ocean temperatures. (Direct radiative forcing from increased atmospheric CO_2 will not affect the meridional structure of an ocean at rest because this forcing is globally uniform.) Salinity was initialized in an equivalent manner. Because this was a high-resolution coupled model and therefore computationally demanding, we focused specifically on the wind-driven circulation in the upper ocean during the late Cretaceous.

The integration period allowed sufficient time for the adjustment of the atmosphere and upper ocean to the increased level of CO_2 and for the establishment of a wind-driven oceanic circulation (which takes on the order of 1 to 10 years to establish) but not for the equilibration of benthic ocean temperatures. We averaged quantities over the last 6 years of the simulation; this procedure eliminated transients of a time scale shorter than 6 years and delivers the robust features of the general atmospheric and oceanic circulation.

The pattern of annual mean wind stress delivered from the atmospheric model (Fig. 1) is similar to that of the present day with modifications as a result of the modified continental geometry (for example, westerly wind stress is reduced over the Indian Ocean as a result of the weaker monsoon).

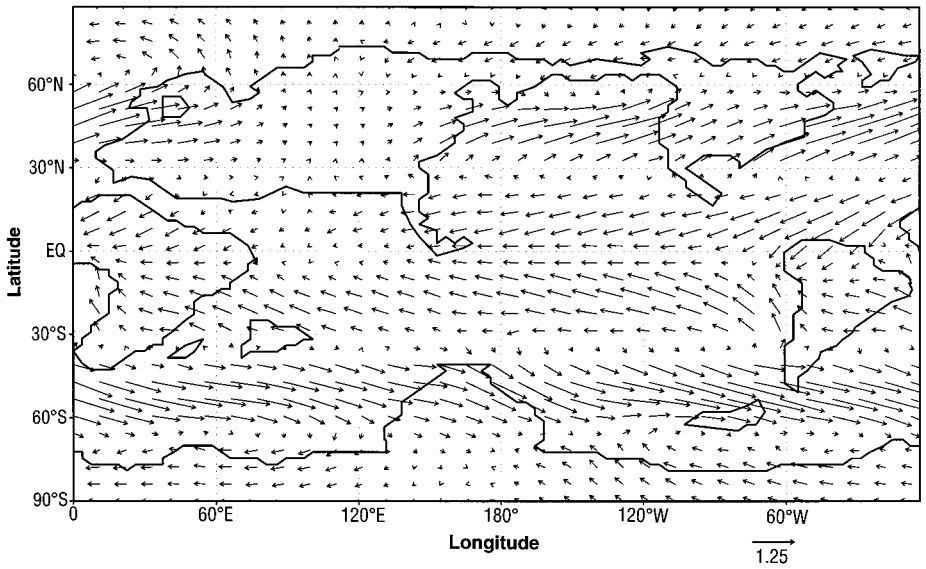

Fig. 1. Annual mean wind stress vectors (in dynes per square centimeter) for the late Cretaceous. Arrows are scaled as displayed in the bottom right. For clarity, vectors are plotted at every third grid point.

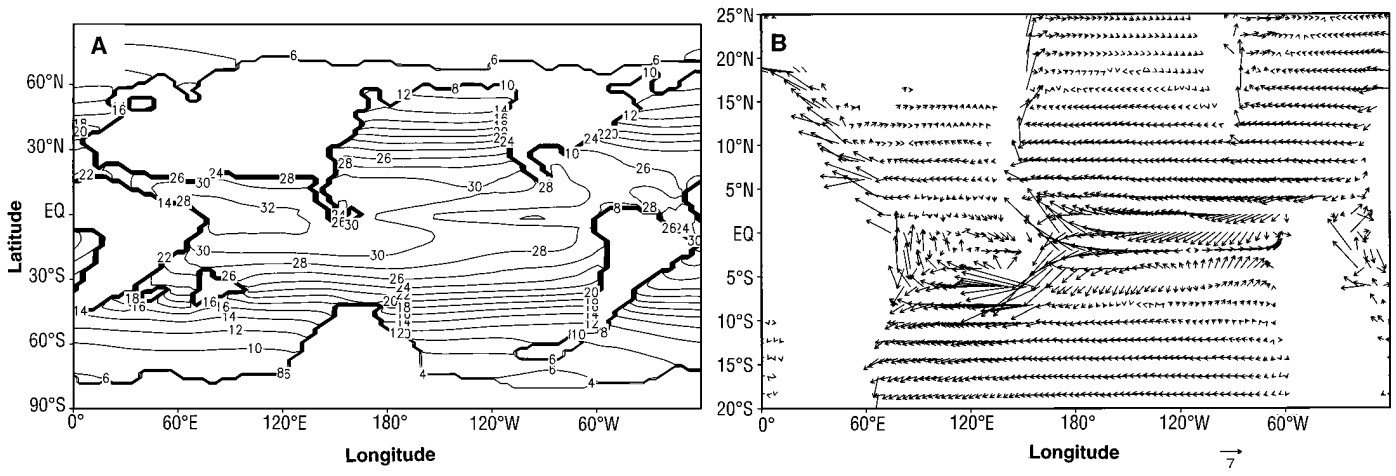

Fig. 2. (**A**) Global annual mean temperature (°C) and (**B**) ocean currents between 20°S and 25°N at a depth of 104 m (shown at this depth to remove the surface Ekman component). The contour interval for temperature is 2°C, and the velocity vectors are scaled in centimeters per second, as shown in the figure.

Winds are easterly in the tropics from 30°S to 30°N and westerly from 35° to 55°N and from 40° to 70°S within the mid-latitude tropospheric jets. In agreement with an earlier atmosphere-only integration for the mid-Cretaceous (*17*), there is no poleward shift of the mid-latitude westerlies in response to an ice-free planet. A June-July-August monsoon occurs in our Cretaceous simulation, with maximum westerly wind speeds of ~10 m/s over the south Eurasian coast. These winds, as is the case for the present-day monsoon, result in anomalously high rates of precipitation in the model (on the order of 1.2 cm/day) over the Cretaceous Indonesian peninsula.

The winds drive gyre circulations in the large ocean basins that are quite similar to those of today's oceans. Cretaceous analogs of the Gulf Stream and Kuroshio close the circulations in the Tethys and north Pacific basins, respectively (Fig. 2). The easterly wind stress that dominates in latitudes below 30°, in conjunction with the open ocean gateways between the Indian, Tethys, and Pacific ocean basins, drives a circumglobal, westward-flowing current whose flow path is similar to that proposed in paleobiogeographical reconstructions (*4*). The current flows along the equator in the Pacific Ocean, around the southern end of the Indonesian peninsula, into the Tethys Seaway between Africa and Eurasia, into the southeastern Tethys Ocean where it is driven southwestward by the local wind stress along the northwestern coasts of Africa and South America, and finally back into the Pacific Ocean through the oceanic gateway between North and South America. We will refer to this current as the TCC. In the southwestern Tethys Ocean, the western Pacific, and the western Indian Ocean, fractions of the TCC diverge to the Gulf Stream, the Kuroshio, and the Agulhas western boundary currents, respectively. Conversely, mass in the simulated TCC is gained by inflow from the broad but weak eastern boundary currents off the west coasts of North and South America and Eurasia.

Our results indicate that the presence of the TCC is not dependent on a poleward shift of the westerly trade winds during the Cretaceous. The current is possible even if the winds at that time were similar to the winds of today. The absence of a TCC in the model of Barron and Peterson (*9*) should be attributed not to incorrect winds in their model but to the relatively low resolution of their ocean model and possibly to the mid-Cretaceous continental configuration. Higher resolution in an ocean GCM permits simulation of less viscous flow, especially in currents that are relatively narrow compared to the grid spacing in the model (such as equatorial, coastal, and western boundary currents). In addition, the continental geometry, in conjunction with the predicted pattern of wind stress, dictates the direction of the current's flow. A somewhat different continental configuration, such as that for the mid-Cretaceous used by Barron and Peterson, may change the structure of the TCC if the model resolution is sufficient to capture the current in narrow seaways.

The path of our simulated TCC makes its most radical and arguably its most biologically important subtropical excursion along the northern coast of Africa, as it flows through the narrow Tethys Seaway between Africa and Eurasia, bringing warm, tropical water northward. As a result, seasonal temperatures in western Eurasia should not have dropped below freezing west of 75°E. In the model, evaporation rates in excess of precipitation rates over the Tethys Seaway induced values of sea surface salinity as high as 37 parts per thousand in the region bordering southwestern Eurasia and north Africa. If real, such high values of salinity in the warm current would have limited the habitability of nearby

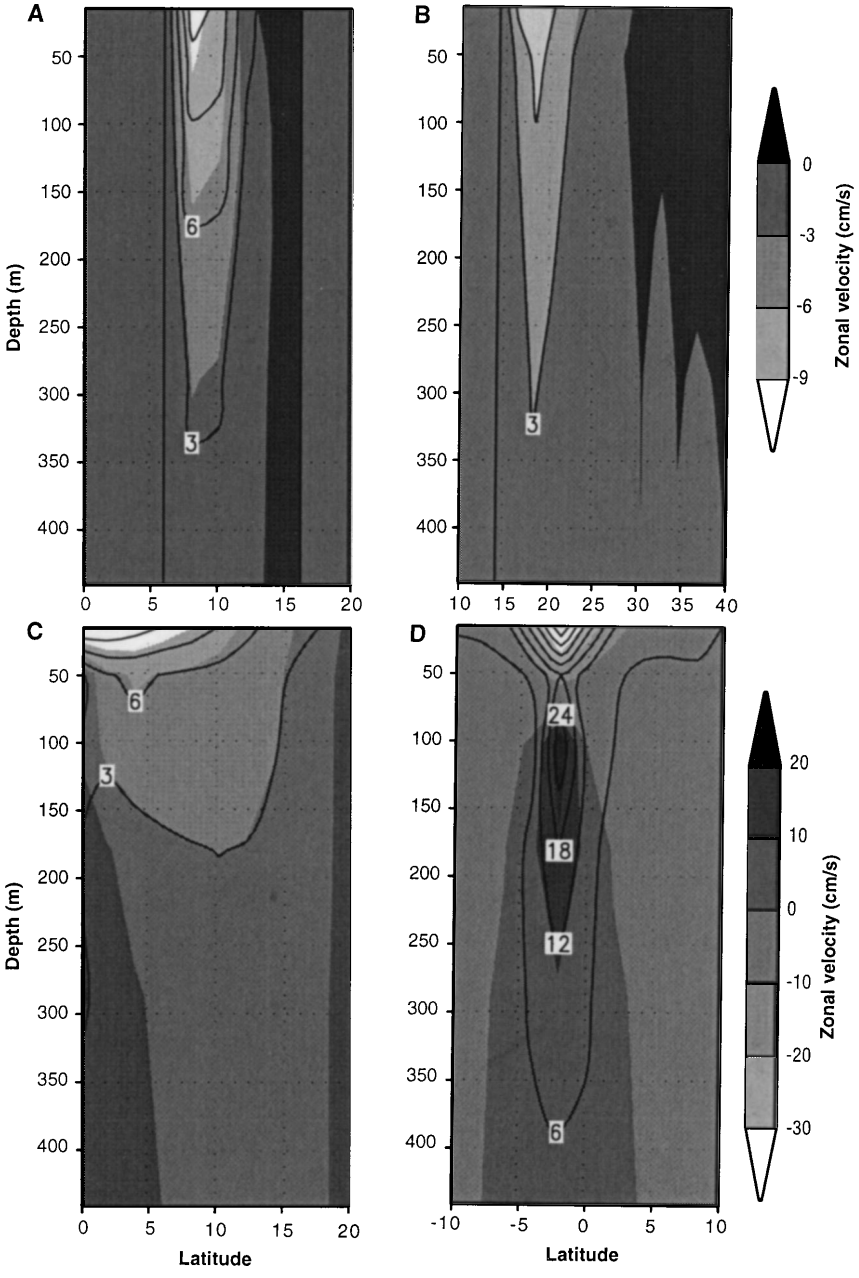

Fig. 3. Depth-latitude plots of the annual mean TCC at various sites around the globe: (**A**) 50°E, (**B**) 0°E, (**C**) 50°W, and (**D**) 180°W. Zonal velocity (shaded) indicates the direction of the current, with lighter colors indicating westward flow. The upper scale bar is for (A) through (C). Contours are of horizontal velocity magnitude, with a contour interval of 3 cm/s for (A) through (C) and 6 cm/s for (D).

coastal regions. The simulated current, upon entering the subtropical Tethys Ocean, is driven back into the tropics and into the Pacific Ocean by strong northeasterly wind stress (see Fig. 1).

In the model, the mean depth of the TCC varies substantially, depending on the width of the channel in which it flows (Fig. 3). In the narrow Tethys Seaway, the TCC attained its maximum vertical extent of ~350 m, whereas in the broad Pacific basin, its vertical scale was less than 100 m (basin depths would therefore need to be of order 100 m for such a surface current to be seriously affected by bathymetry in a stratified ocean). The half-width of the TCC had its smallest value of 440 km in the Tethys Seaway and in the equatorial Pacific basin; its largest value of 1540 km was in the southern Tethys Ocean off the northern coast of South America. The predicted core velocity of the TCC ranged from ~43 cm/s in the Pacific to ~11 cm/s in the Tethys Seaway and Ocean. These parameters deliver a mass flux of 17 sverdrup in the Tethys Seaway, 29 sverdrup in the southern Tethys Ocean, and 13 sverdrup in the Pacific basin.

In such a relatively narrow channel as the Tethys Seaway, however, the surface currents might be strongly influenced by the seasonal south Eurasian monsoon, which in the present-day climate induces surface current reversals (from westward to eastward) off the northeast coast of Africa during the Northern Hemisphere summer. The simulated currents in the Tethys Seaway during June, July, and August (Fig. 4) do indeed display a reversed, eastward-flowing monsoon current near the surface. However, this current reversal occurs along the south Eurasian coast and does not countercheck the westward flow of the TCC. The TCC is 5 cm/s weaker than the annual mean during these monsoon months but remains a robust feature of the simulation. However, an increase of mixing and eddy kinetic energy through shear instability between the westward TCC and the eastward monsoon current should occur during the northern summer, as well as coastal upwelling along the south Eurasian coast, which may account for the geological evidence of coastal upwelling in the region (*7*).

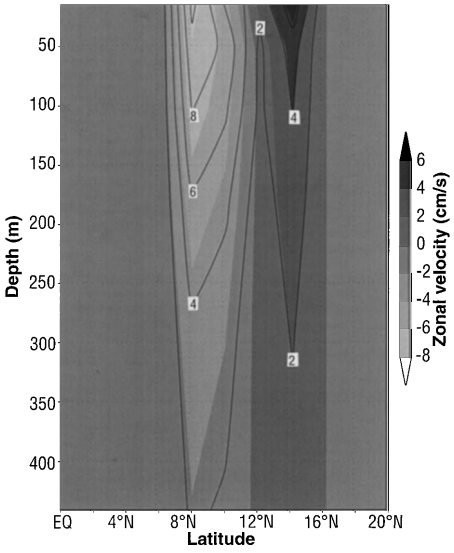

Fig. 4. Depth-latitude plots of the annual mean TCC at 50°E, as in Fig. 3A, but averaged over the Northern Hemisphere monsoon months of June, July, and August. The horizontal-velocity contour interval is 2 cm/s.

REFERENCES AND NOTES

1. A. Hallam, in *An Outline of Phanerozoic Biogeography*, A. Hallam, B. R. Rosen, T. C. Whitmore, Eds. (Oxford Univ. Press, Oxford, 1994), pp. 178–203.
2. F. Rogl and F. F. Steininger, in *Fossils and Climate*, P. Brenchley, Ed. (Wiley, New York, 1984), pp. 171–200.
3. B. P. Luyendyk, D. Forsyth, J. D. Phillips, *Geol. Soc. Am. Bull.* **83**, 2649 (1972); W. A. Gordon, *J. Geol.* **81**, 269 (1973).
4. B. U. Haq, in *Marine Geology and Oceanography of Arabian Sea and Coastal Pakistan*, B. U. Haq and J. D. Milliman, Eds. (Van Nostrand Reinhold, New York, 1984), pp. 201–231.
5. S. M. Stanley, *J. Paleontol.* **69**, 999 (1995); A. Hallam, in (*2*), pp. 107–125.
6. C. M. Janis, in (*2*), pp. 85–104.
7. K. B. Föllmi and M. Delamette, *Science* **251**, 94 (1991); E. J. Barron and W. H. Peterson, *ibid.*, p. 94.
8. E. J. Barron and W. H. Peterson, *ibid.* **244**, 684 (1989).
9. ———, *Paleoceanography* **5**, 319 (1990).
10. E. J. Barron and W. Washington, *J. Geophys. Res.* **89**, 1267 (1984).
11. C. T. Gordon and W. Stern, *Mon. Weather Rev.* **110**, 625 (1982).
12. R. C. Pacanowski, K. Dixon, A. Rosati, *GFDL Ocean Group Tech. Rep. 2* (Geophysical Fluid Dynamics Laboratory, Princeton, NJ, 1991).
13. S. Manabe and K. Bryan Jr., *J. Geophys. Res.* **90**, 11689 (1985).
14. S. Manabe and R. J. Stouffer, *Nature* **378**, 165 (1995).
15. P. A. Sandberg, *ibid.* **305**, 19 (1983).
16. A. M. Ziegler, C. R. Scotese, S. F. Barrett, in *Tidal Friction and Earth's Rotation II*, F. Brosche and J. Sundermann, Eds. (Springer-Verlag, Berlin, 1982).
17. E. J. Barron and W. Washington, *Geology* **10**, 633 (1982).

18. The author gratefully acknowledges the support of a University Corporation for Atmospheric Research Postdoctoral Fellowship in Ocean Modeling, as well as G. Philander for making this work possible.

30 October 1996; accepted 27 December 1996

Structure of DNA–Cationic Liposome Complexes: DNA Intercalation in Multilamellar Membranes in Distinct Interhelical Packing Regimes

Joachim O. Rädler,* Ilya Koltover, Tim Salditt, Cyrus R. Safinya†

Cationic liposomes complexed with DNA (CL-DNA) are promising synthetically based nonviral carriers of DNA vectors for gene therapy. The solution structure of CL-DNA complexes was probed on length scales from subnanometer to micrometer by synchrotron x-ray diffraction and optical microscopy. The addition of either linear λ-phage or plasmid DNA to CLs resulted in an unexpected topological transition from liposomes to optically birefringent liquid-crystalline condensed globules. X-ray diffraction of the globules revealed a novel multilamellar structure with alternating lipid bilayer and DNA monolayers. The λ-DNA chains form a one-dimensional lattice with distinct interhelical packing regimes. Remarkably, in the isoelectric point regime, the λ-DNA interaxial spacing expands between 24.5 and 57.1 angstroms upon lipid dilution and is indicative of a long-range electrostatic-induced repulsion that is possibly enhanced by chain undulations.

Somatic gene therapy depends on the successful transfer and expression of extracellular DNA to the nucleus of eucaryotic cells, with the aim of replacing a defective or adding a missing gene (*1*). Viral-based carriers of DNA are presently the most common method of gene delivery, but there has been a tremendous activity in developing synthetic nonviral vectors (*2*). In particular, cationic liposomes (CLs) (*3*), in which the overall positive charge of the cationic liposome-DNA (CL-DNA) complex enhances transfection by attaching to anionic animal cells, have shown gene expression in vivo in targeted organs (*4*), and human clinical protocols are ongoing (*5*). Cationic liposome transfer vectors exhibit low toxicity, nonimmunogenicity, and ease of production, but their mechanism of ac-

Materials Department, Physics Department, and Biochemistry and Molecular Biology Program, University of California, Santa Barbara, CA 93106, USA.

*Present address: Physikdepartment, Technische Universität München, Institut für Biophysik (E22), James Franck–Strasse, 85747 Garching, Germany.
†To whom correspondence should be addressed.